

Particle ID performance of Liquid Argon TPC

J-PARC T32 collaboration

Abstract

This paper describes a study of particle identification performance of liquid Argon TPC (LArTPC) detector using well-defined charged particles (pions, kaons, and protons) with momentum of $800 \text{ MeV}/c$ obtained at J-PARC K1.1Br beamline.

We have build a LArTPC detector with fiducial mass of 150 kg , and injected the beam particle

Keywords:

1. Introduction

Refer [1] for hardware/beam line description

2. Data Quality

2.1. Collected Data

Table 1 shows list of the collected data while Oct/2010 Run. 800 MeV/ c pion is expected to pass-through the detector as MIP, and have uniform energy deposition to all the TPC channels. So this data set is very useful for calibrating the detector response (See section xxx). 800 MeV/ c proton stops after 15 cm of flight distance inside the TPC fiducial volume with relatively large dE/dx . So we use the proton data set for validation of the detector response at high dE/dx region(See section xxx). We have collected three different Kaon data by varying thickness of the degrader. 540, 630, 680 MeV/ c are corresponds to the momentum degraded by 2 lead glass, 1 lead glass + 1 lead block, and 1 lead glass, respectively, and such Kaon stops after 10 cm, 50 cm, and 65 cm of flight distance inside TPC fiducial volume.

Figure 1 shows an 2D display of typical event taken with 800 MeV/ c electron trigger. Horizontal axis corresponds to TPC channel number and zero means most upper stream strip. Since strip pitch is 1 cm, this is equivalent to distance from beam injection point in cm. Vertical axis corresponds to electron drift time in μs and $t=0$ means trigger timing. In this TPC, anode and cathode is located at top and bottom of the detector, respectively, $t=0$ means energy deposition at anode and longer drift time means energy deposition in lower height. With 200 V/cm of electric field, drift velocity is about 0.8 m/ms. So drift of full detector (40 cm) takes 500 μs . Color strength of the plot corresponds to the TPC signal pulse height in ADC counts which is roughly proportional to dE/dx of the track. In this event, triggered electron can be clearly seen center of the detector as an electromagnetic shower while there are two other particles accidentally overlapped with the triggered electron. Track at $t=100 \mu s$ is considered as a proton which stops after 15 cm of flight distance and has large dE/dx around the stopped point. Track at $t=400 \mu s$ is considered as a pion which passes-through the detector and has uniform dE/dx over the TPC channels. This event already gives us some idea for how good the particle identification performance of the LArTPC is.

Figure 2 shows a typical $K \rightarrow \mu\nu$ like event. We can clearly identify a kink of the track at 60 cm which is considered as stopped point of Kaon and it decays to

Energy deposition of the track is about MIP at the injection point and gradually increase towards the stopped point at 60 cm.

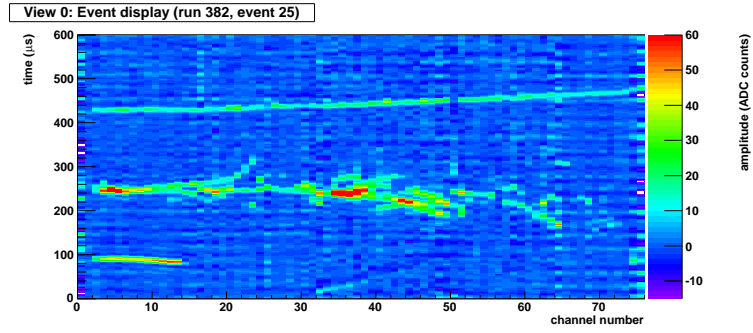


Figure 1: Event display of 800 MeV/ c electron triggered event. Accidentally overlapped with a proton and a pion.

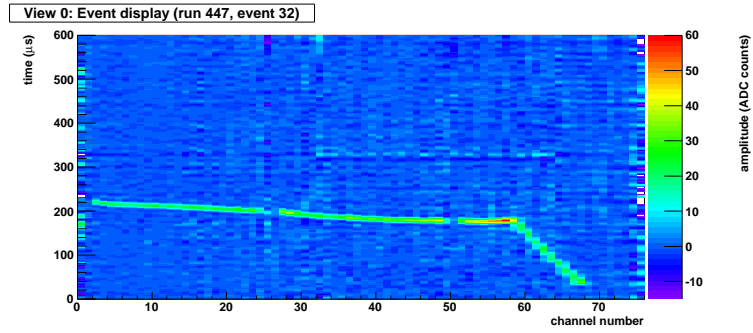


Figure 2: Event display of Kaon 630 MeV/ c triggered event

Table 1: List of collected data		
Particle	Momentum (MeV/c)	Number of Events
Pion	800	3,000
Proton	800	1,500
Kaon	540 (2LG)	7,000
Kaon	630 (1LG+1LB)	40,000
Kaon	680 (1LB)	35,000
electron	800	2,500
electron	200	10,000
pion	200	10,000

2.2. Beam Quality

As described in section xx, we have several beam counters to indentify beam particles event by event(see Fig3).Using this when taking data, we can get data of interest selectively.The following describe how to identify beam particles with the typical data (Data Name:PhysicsOct48) including K^+ , π^+ , e^+ , p events, and their momentum adjusted $\sim 800\text{MeV}/c$.

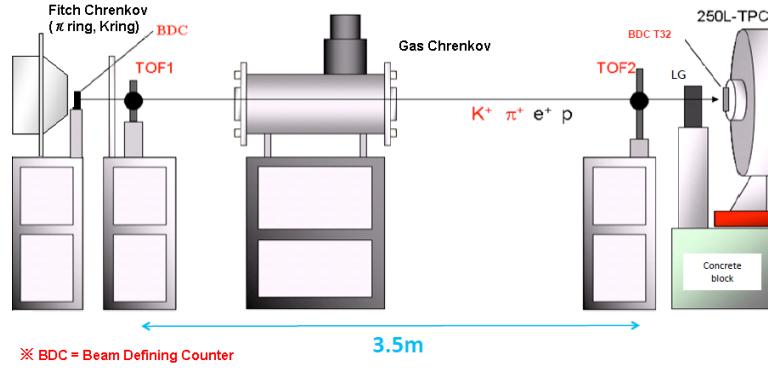


Figure 3: Instruments on K1.1BR Beam Line

Leaded particles to K1.1BR beamline pass the Fitch Cheernkov Counter. Fitch Cherenkov Counter can select particles with differences of angle of cherenkov light which they radiate. Fiture4 shows response of the Fitch Cherenkov Counter. The horizontal axis shows the total amount of PMT signal where cherenkov light of $800\text{MeV}/c$ π can be detected. The vertical

axis shows that of 800MeV/c K . Signal are distinctly seperated to three cluster and can be categorized as following.

1. FC Signal(π)<1450 & & FC Signal(K)>2000
2. FC Signal(π)<1450 & & FC Signal(K)<2000
3. FC Signal(π)>1450 & & FC Signal(K)<2000

Apparently, particles within the region 1 are K^+ candidates. Particles within region 2 are p candidates because 800MeV/c p is impossible to radiate cherenkov light. Particles within region 3 are π^+ or e^+ candidates because angle of cherenkov light are the same level.

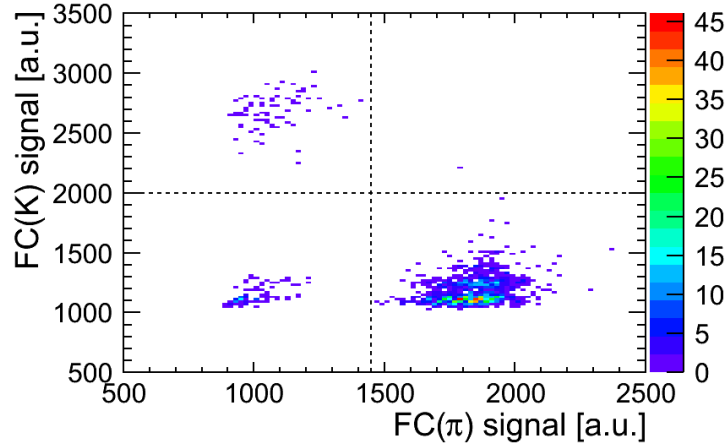


Figure 4: Fitch Cherenkov Counter

Next, beam particles passed the TOF Counter. There are two TOF Counters whose distance is 3.5m, and each particles can be separated with the difference of time of flight between them. Following table2 is calculated time of flight when each 800MeV/c particles passes two conters.

Figure5 shows responce of the TOF Counters. The horizontal axis shows the difference of time information between TOF1 and TOF2 Counter. However, because the timing of zero of time infomation isn't matched between

particle	e^+	π^+	K^+	p
Mass(MeV)	0.511	139.57	493.68	938.27
Time of Flight(ns)	11.67	11.84	13.71	17.98

Table 2: Time of flight of each particles

them, the horizontal axis are shifted parallel from the real time of flight. The vertical axis shows the number of events. Signal have clearly divided structure and can be categorized as following. From table2, the region1 include e^+ or π^+ candidates, and the region2 include K^+ candidates, and the region3 include p candidates.

1. Time of Flight < the value added 4.5σ to the mean of the left structure
2. above boundary value < Time of Flight < 8.75 (because of the clear separation from the right structure)
3. Time of Flight > 8.75

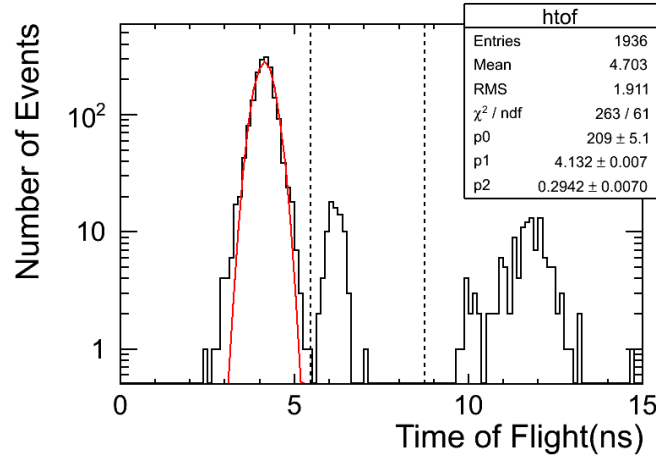


Figure 5: TOF Counter

Fitch Cherenkov Counter and TOF Counter can't identify e^+ and π^+ . However, Gas Cherenkov Counter can detect e^+ because the gas in this detector has the refractive index only e^+ can radiate cherenkov light. Figure6

Data Name	e^+	π^+	K^+	p	<i>uncertain</i>	Number of Events
PhysicsOct42	68	1617	27	232	5	1949
PhysicsOct48	128	1594	78	126	11	1937
PhysicsOct49	0	341	0	1146	12	1499
PhysicsOct52	0	1	3126	0	76	3203
PhysicsOct55	0	6	8386	0	208	8600
PhysicsOct59	0	8	5863	0	119	5963
PhysicsOct60	0	1	1870	0	40	1911

Table 3: Beam components of data ued for analysis

shows response of the Gas Cherenkov Counter. The horizontal axis shows the PMT signal of Gas Cherenkov Counter. Fitting the pedestal with gaussian, the events larger by the value added 3.5σ to the mean of the pedestal is e^+ candidates.

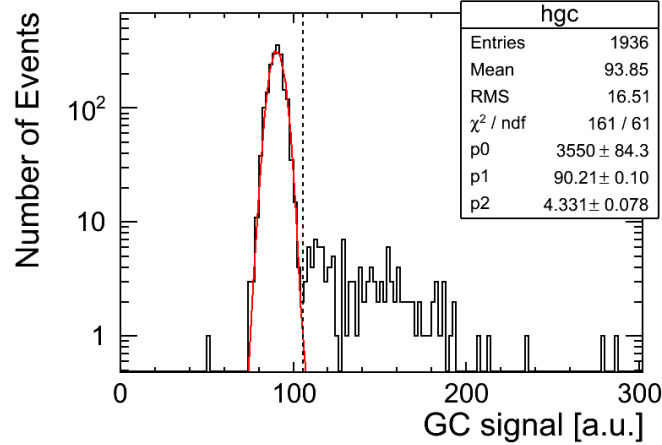


Figure 6: Gas Cherenkov Counter

Particles which satisfy all conditions for the same candidate are identified them, and the others are defined ‘uncertain’ particles. Herewith, we can identify beam particles with high purity before injection to 250L detector. Table2.2 shows the beam components of the data used for analysis. It should be noted that the values used categorization are changed as appropriate.

PhysicsOct52,55,59,60 is the data which was required ‘FC signal(K)<2000’ when taking data for analysis. As table2.2 shows, these data is almost occupied K^+ events and the ratio is $\sim 98\%$ on average.

2.3. Beam Energy

30GeV proton beam hits to target T1 in Hadron hall. It generates many particles like kaon, pion, muon, electron, and so on. We take the particles that has 800MeV/c momentum from this beam by using D1 magnet.

For this analysis, a beam momentum at BDC after passing through the K1.1Br beam line is required. We estimate a beam momentum using simple MC simulation. Figure 10 shows MC simulation’s geometry. This time, beam line is straight and has no electric and magnetic field. MC simulation shoot 800MeV/c kaon and pion as pencil beam.

Figure 11 shows kaon and pion momentum distribution using this MC simulation. Actually, kaon momentum distribution peak is adjusted so that kaon decay point of MC simulation is consistent with data. Section 2.3.1 explains this point. And proton momentum is estimated in other way, using TREK detector TOF information. Section 2.3.2 shows proton momentum distribution.

2.3.1. Kaon energy

We adjust momentum peak of figure ?? and set Kaon beam energy the point that the decay points of Kaon in data and simulation are good agreement. The distribution of decay points are plotted in Figure7.

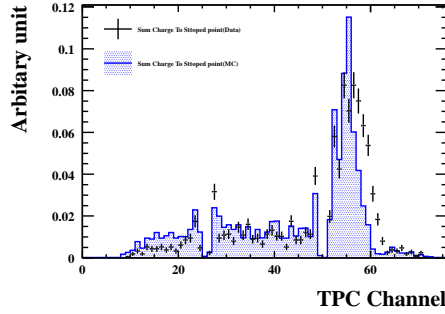


Figure 7: Decay point distribution of Data and MC

2.3.2. Proton energy

Beam momentum is ideally TOF information, but considering the dispersion, we should take into account of the resolution of TOF. As we know the resolution of TOF is $\sim 200\text{ps}$ beforehand, we can calculate the effect of this resolution to beam momentum. For example, as shown in table 2, the time of flight of $800\text{MeV}/c$ K^+ between two TOF Counters is 13.71ns . When considering 0.2ns TOF resolution for this value, the momentum is approximately $760\sim 845\text{MeV}/c$ spreading largely. However, taking the same calculation for $800\text{MeV}/c$ p , the momentum is approximately $785\sim 815\text{MeV}/c$ suppressing the dispersion to some extent. In addition, because the dispersion of Time of Flight of p appears widespread over TOF resolution, we estimate the momentum of p from TOF information.

Figure 8 shows response of TOF Counters of PhysicsOct49 whose data include many p events. As described above, the horizontal axis doesn't show the real time of flight. Then, with PhysicsOct47 whose data include much e^+ events, we determined the mean of e^+ . As the β of e^+ is ~ 1.0 , this value of horizontal axis corresponds to 11.67ns (dotted line in Fig 8). Figure 9 shows the estimated momentum histogram from Figure 8 and this momentum distribution is implemented to Monte Carlo Simulation. Whether the distribution reproduces DATA well is discussed in section 7.2.

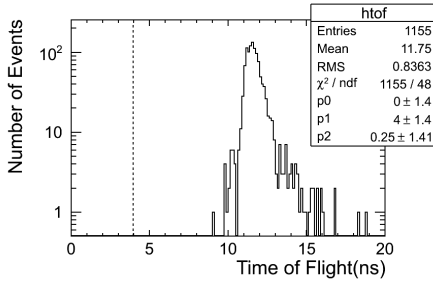


Figure 8: p TOF response

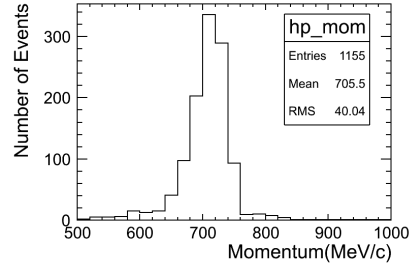


Figure 9: Estimated p momentum

2.3.3. Energy deposition in degrader

Because of having high energy, kaon beam from BDC passes through 250LAr TPC. So that kaon stops in 250LAr TPC, we put degrader, which reduces beam energy, on beam line. In this experiment, we used lead glass and lead block as degrader. We estimate energy deposition in degrader by using MC simulation. Figure 12 shows energy deposition in degrader.

2.4. Beam Position

Before taking data, we measured a beam profile on the front of 250LAr TPC by using plastic scintillation counter. Figure 13 shows beam profile on the front of 250LAr TPC.

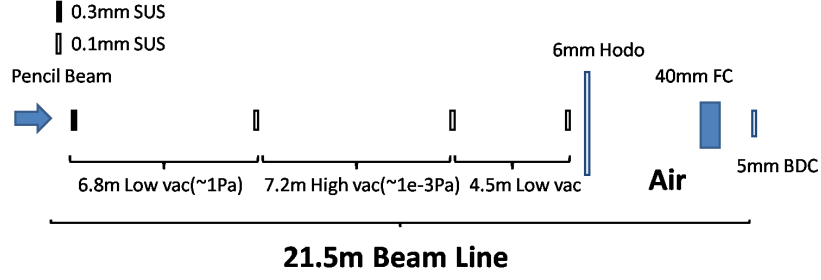


Figure 10: K1.1 Br beamline

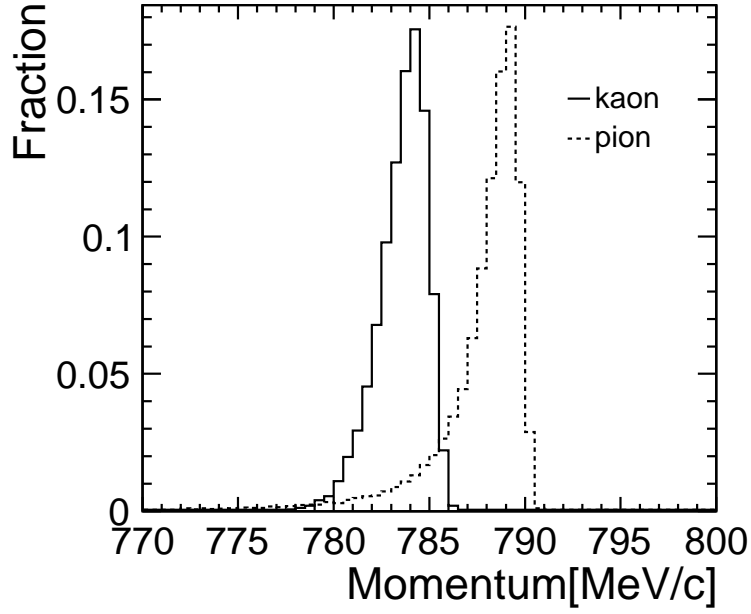


Figure 11: kaon and pion momentum distribution at BDC

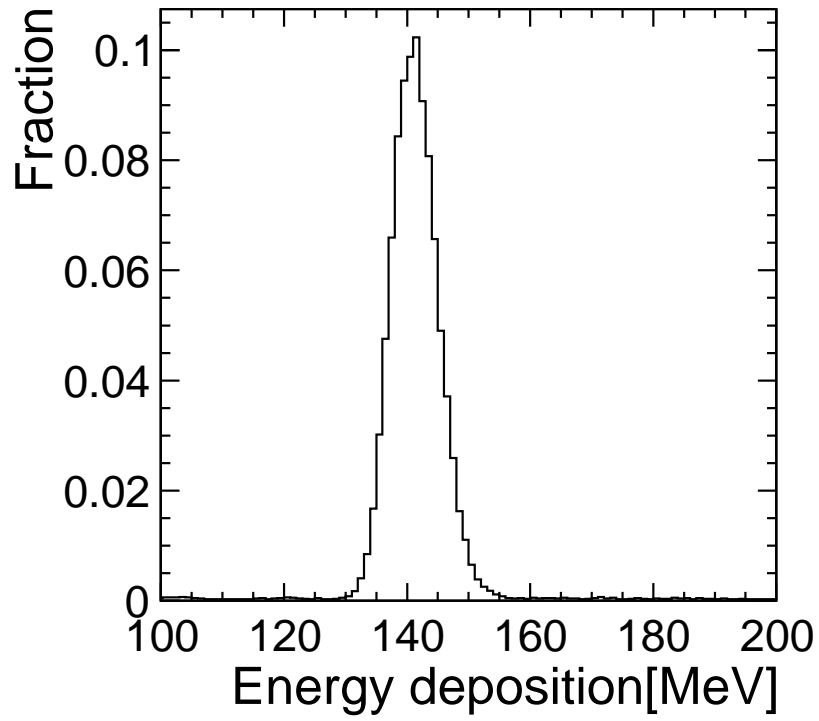


Figure 12: energy deposition in degrader

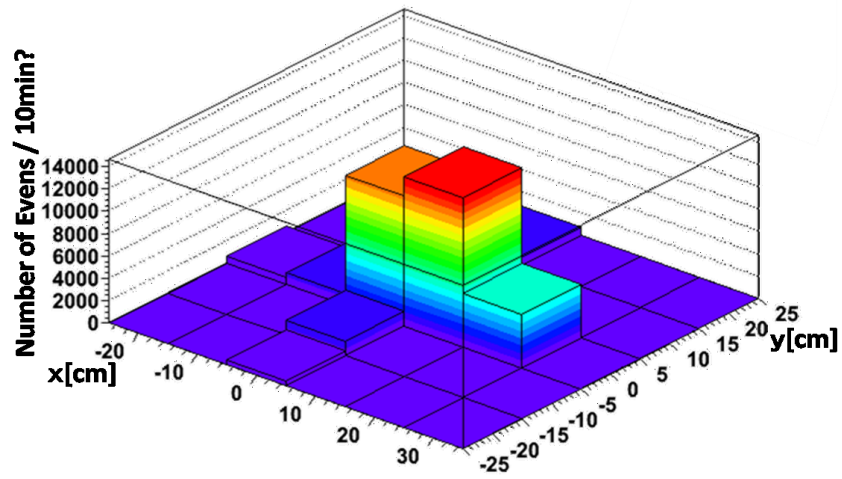


Figure 13: Beam profile on the front of 250LAr TPC

3. Software Framework

Qscan is a general purpose software package for LArTPC analysis(reference) which provides,

- event reconstruction: noise reduction, hit finding, clustering, and tracking...
- event simulation: GEANT VMC with ROOT geometry, ionization electron recombination, drift, digitization...
- event visualization: display raw data waveform and reconstructed quantities

4. Event Reconstruction

4.1. Noise Reduction

Figure 15 shows raw waveform of the TPC signal before applying any noise reduction. Two waveforms shown in this plot are channel 13 and 37 in Figure 1 which are roughly proton stopped point and electron shower maximum point, respectively. Signal-to-noise ratio for this particular case is poor and pion signal which is supposed to be $t=400 \mu s$ is almost hidden by the noise. While time width of TPC signal is few μs which is determined by drift time between anode and anode-grid, dominant noise component looks higher frequency. To reduce such noises, we have applied FFT (Fast Fourier Transformation) filter to cut the high frequency component. Figure ?? shows amplitude as a function of frequency for the same event. This clearly shows dominant noise component with > 200 kHz has good separation with signal component (< 100 kHz). Figure 16 shows the waveform after removing high frequency (> 80 kHz) component by the FFT filter. Signal-to-noise ratio is dramatically improved. On the other hand, we expect certain bias to the signal charge measurement by this filter, and it will be discussed in Section X.

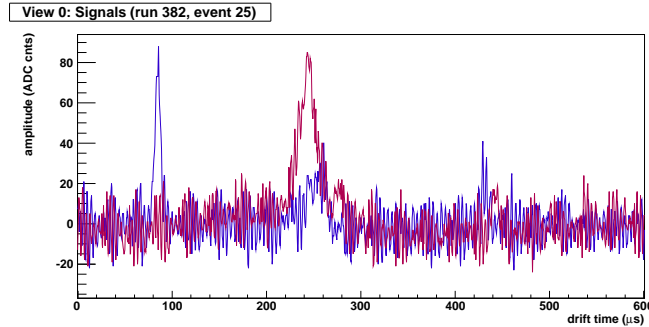


Figure 14: TPC raw signal waveform for "Textbook" event channel 13 and 37.

4.2. Hit Finding/Clustering

After noise reduction we find signal hits and create clusters associated to single tracks. Hit is defined as bump over given threshold in a channel. After finding all hits in an event, we construct cluster by merging adjacent hits. The example of hit finding and clustering is shown in Fig 17, which

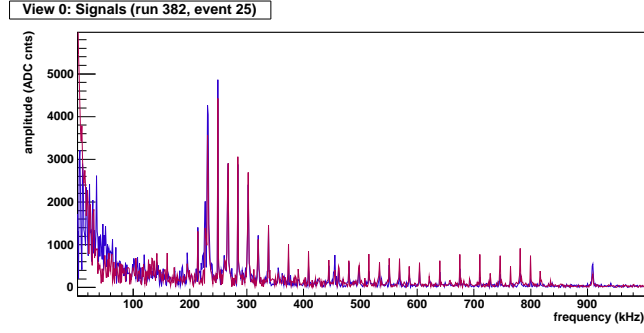


Figure 15: FFT frequency amplitude distribution

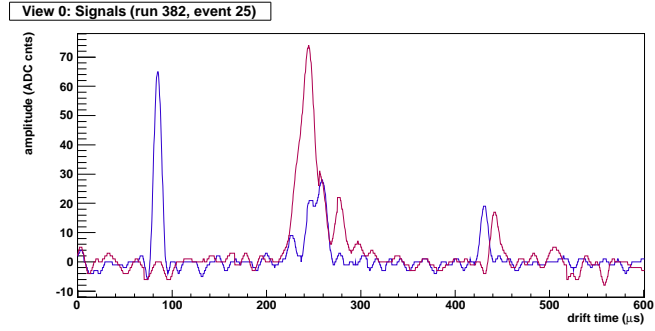


Figure 16: TPC signal waveform after cutting the frequency > 80 kHz.

indicates reasonable hit and cluster findings. Threshold of hit finding is six for our analysis. Monte Carlo simulation shows 99.8% and 81.8% hit finding efficiencies for Kaon and decayed muon hits, respectively. Average noise hits are about 7.5 in an event.

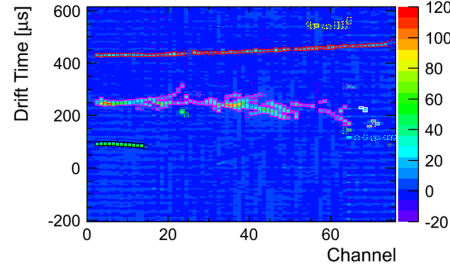


Figure 17: Example of hit finding and clustering. A colored box corresponds to a hit and colors represent different clusters.

- Plot: Finding efficiency vs threshold (Naganoma): TBU
- Plot: Through-going pion data Q vs pion (Tanaka)

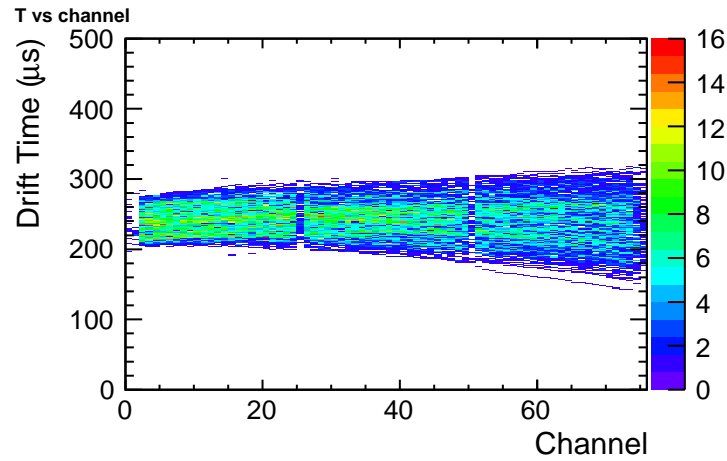


Figure 18: 800 MeV/c pion sample

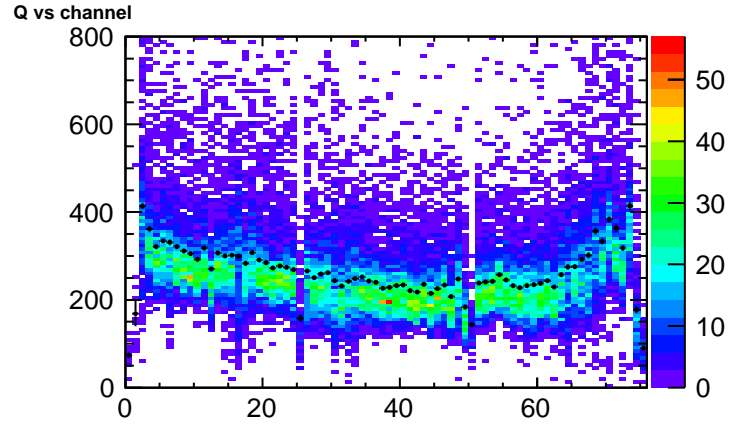


Figure 19: 800 MeV/c pion average hit charge

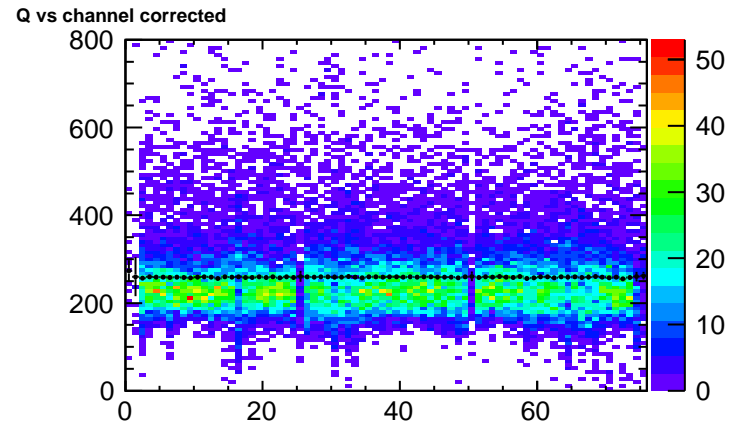


Figure 20: 800 MeV/c pion average hit charge after calibration

4.3. Stopped Point Finding

4.3.1. Proton

Figure 21 shows typical EventDisplay of Proton. Proton has simple structure of events, that is, as Proton doesn't decay any particles, so it is easy to define stopped point.

First, We define 'max channel' and 'max charge channel' event by event (then, required single cluster for single event). 'Max channel' is the channel number of hit which has the most large channel number in the cluster, and 'max charge channel' is the channel number of hit which has the most large amount of signal. We select events in either following two situations, and define 'max channel' as stopped point.

- max channel = max charge channel
- max channel = max charge channel + 1

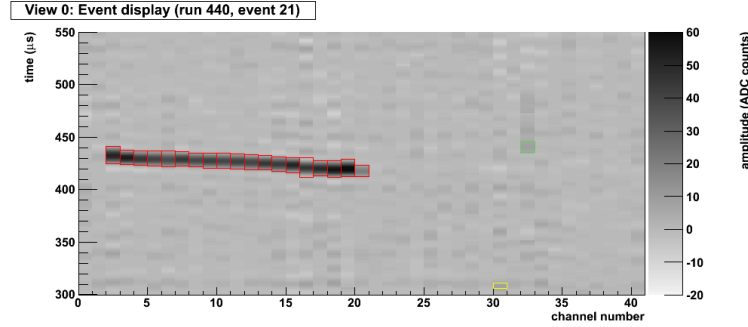


Figure 21: Typical Event Display of Proton

4.4. Stopped Kaon

Hough transform was invented for machine analysis of bubble chamber photographs by Paul.V.C.Hough.[6] We detect straight lines using hough method, and find Kaon stopped point from the intersection of straight lines. Figure 22 shows hit map like a Kaon track. One point in the X-Y space can be transformed into sinusoidal curve in the ρ - θ space. Figure 23 shows sinusoidal curves in all points. And, we detect the straight line associated

with the largest number of points by choosing the most dense point in ρ - θ space. Next , the sinusoidal curves of the hits associated with first straight line are removed from figure 23. Figure 24 shows sinusoidal curves after the hits associated with first straight line removed. We detect second straight line using the same procedure. This procedure is repeated until there are less than three points. Figure 25 shows the two straight lines detected by hough transform method.

Kaon stopped point in the liquid argon detector defined as charge maximum point around the intersection of some lines.

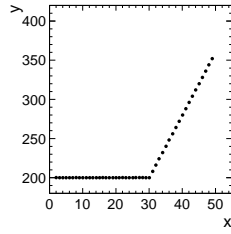


Figure 22: Hit map like a Kaon track

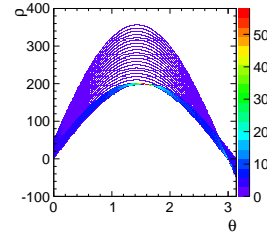


Figure 23: sinusoidal curves getting from all hough transformed points of Figure 22

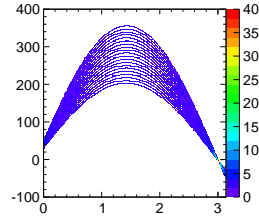


Figure 24: sinusoidal curves removed the points associated with first straight line from figure 23

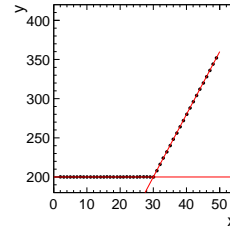


Figure 25: Two lines detected with hough transform method

4.4.1. Chi2 method

χ^2 method is the algorithm that search the point of rapidly increasing fit' χ^2 and the point defined as the stopped point. Because the charged particle coming from upstream of beam line , track reconstruction is started from minimum channel to the maximum channel of the cluster.

Figure 26 shows hit map like a Kaon track. We start fitting with straight line from minimum channel to maximum channel. Figure 27 shows range vs fit χ^2 distribution. As it can be noticed for figure 27, χ^2 is increased rapidly if the straight line is strayed out. Then, we search the strayed point from the straight line by setting reasonable threshold and draw from minimum channel to the strayed point. This procedure is done from maximum channel to minimum channel in the same way. And we draw from maximum channel to the strayed point. Kaon stopped point in the liquid argon detector defined as charge maximum point around the intersection of two lines.

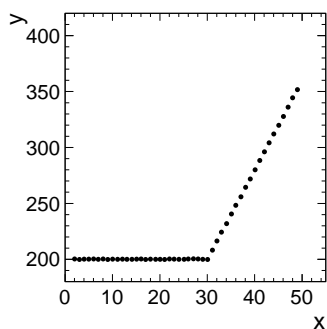


Figure 26: hit map like a Kaon track

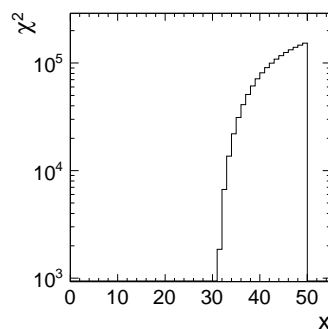


Figure 27: range vs χ^2 distribution

4.4.2. BS method

In the χ^2 method, we can't detect Kaon stopped point in the case of backward decay. Then, we detect Kaon stopped point using BS method. BS method is concept that the Kaon stopped point defined as lightmost channel in the case of backward decay. we describe below how the track defined as backward decay. N_1 is defined as Number of cluster hits found by the clustering. Stopped point finding is started from minimum channel. We search for the closet timing hit in next channel from current channel hit. Then, we repeat this procedure until maximum channel and count the number of selected hit information (N_2). In the case of backward decay, N_1 is larger than N_2 . So, we set reasonable threshold of the difference between N_1 and N_2 , and if the $N_1 > N_2$ is over the threshold, the track is defined as backward decay. In the case of backward decay, we defined charge maximum point around the maximum channel as the stopped point.

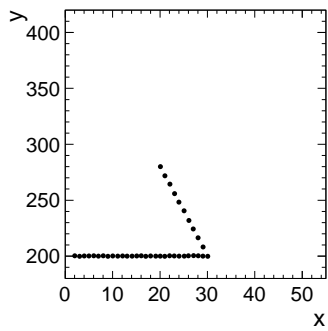


Figure 28: hit map like a Kaon track

5. Liquid Argon Purity

Attenuation of the drift electron depends on purity of LAr since electronegative impurities capture it [5]. Thus we need to apply correction to TPC signal charge depends on the drift time. We use cosmic ray sample triggered by inner PMT at off-beam timing for measuring the LAr purity, and use this to correct the beam data. Figure 29 shows an event display of typical cosmic muon event across TPC channels. The attenuation of readout charge depending on drift time is clearly seen in the right plot. Readout charge in an event cannot be fitted by exponential because energy deposition follows Landau distribution and charge readout is affected by electric field distortion which is described latter in section ??.

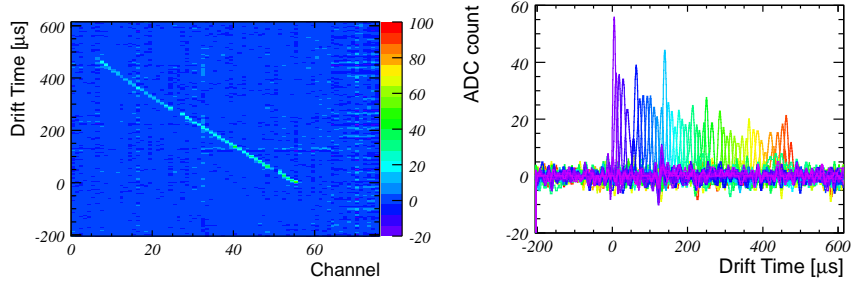


Figure 29: Left: Typical cosmic muon event across TPC channels. Right: Charge deposit as a function of drift time. Colors correspond to different TPC channels.

We select cosmic ray event with more than 20 TPC channels which corresponds to zenith angle of more than 27° and consistent with straight line by χ^2 fit. Readout charge is corrected for field distortion and projected to beam direction to correct injection angle. We fit readout charge by Landau function in each drift time bin to estimate average charge deposit. Figure 30 shows example of the average readout charge as a function of drift time is fitted by exponential to obtain drift electron lifetime. Realistic Monte Carlo simulation shows about 13% (TBU) smaller lifetime estimation due to noise, field distortion, and FFT effects. We correct output lifetime from these effects. Figure 31 shows an drift electron lifetime as a function of duration after initial LAr filling. Drift electron lifetime was $600 \mu\text{s}$ at 60 hours, and $400 \mu\text{s}$ after 150 hours. The degradation is possibly due to impurity from micro

leak or out-gassing penetrating faster than purification by gas recirculation. But we kept enough drift electron lifetime during data taking period.

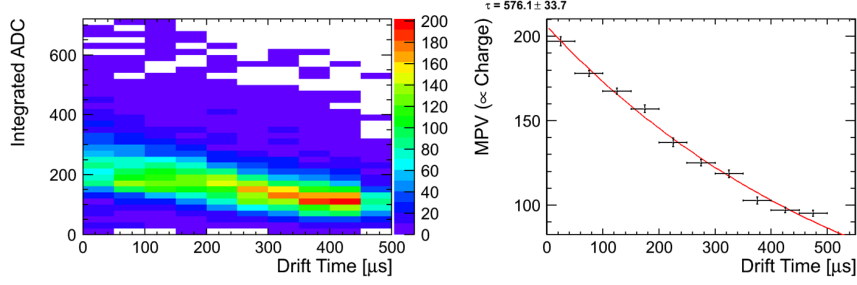


Figure 30: TBU. Left: Readout charge as a function of drift time. Readout charge in each drift time bin is fitted by landau function. Right: Average charge readout as a function of drift time which is fitted by exponential to estimate drift electron lifetime.

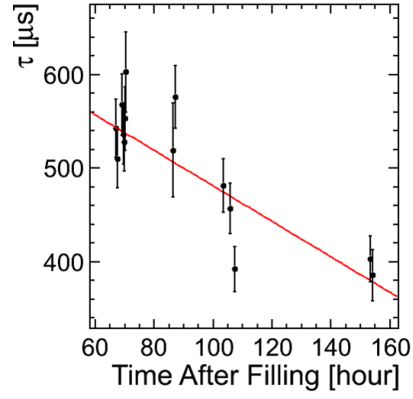


Figure 31: TBU. Drift electron lifetime as a function of duration after initial LAr filling. The lifetime is used to correct the beam data.

6. Event Simulation

6.1. Geant3, recombination, drift velocity

We use GEANT3 for simulating energy deposition of initial beam particles and secondary particles to LArTPC detector and beamline counters.

we set the maximum step of Geant to 0.5 mm which is enough smaller than the readout pitch of 1 cm. It means charge deposition in one strip is typically simulated with 20 GEANT steps.

We set energy cut-off for soft electron/photon emission to 10 keV which is minimum possible energy can be set in GEANT3. This cut-off is very important for ionization electron recombination.

Recombination of electron and Argon ion depends on the electric field and dE/dx . We use a measurement in Ref.[3].

$$Q = A \frac{Q_0}{1 + k dE/dx}, A = 0.800, k = 0.486 \quad (1)$$

Velocity of the drift electron depends on the liquid Argon temperature and the electric field. We use a measurement in Ref [4].

- Plot: Geant Geometry, typical track (Tanaka)
- Plot: recombination factor, drift velocity (Tanaka)

6.2. Electric Field

Electric field of the TPC field cage We have calculated the electric field using a 2D FEM (Finite Element Method) package [?].

This field map is used for simulating electron drift.

6.3. Drift Electron Diffusion

- Plot: drift simulation (Tanaka)

6.4. Preamplifier Gain Calibration

- Preamplifier gain vs channel number (Naito)

6.5. FFT Noise

Adding realistic noise to MC simulation is very important. In this section, we will introduce how to make realistic noise and implement to MC.

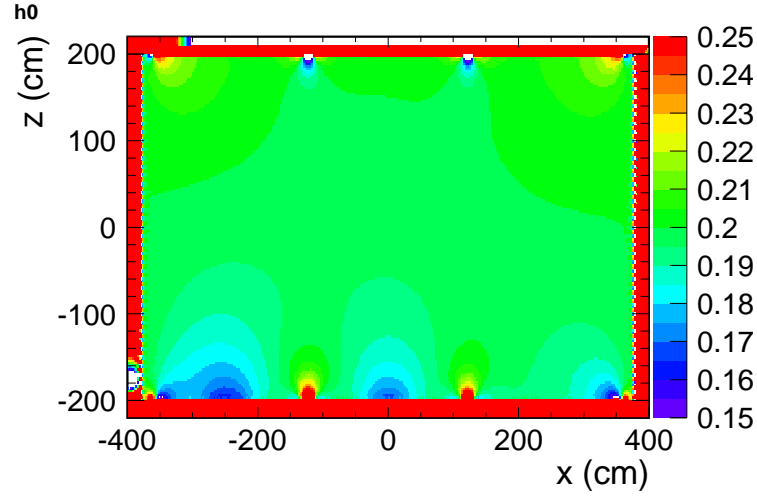


Figure 32: Electric field map obtained from 2D FEM calculation

6.5.1. Noise information of Real DATA

As a first step, we checked distribution of frequency from real data using FFT(Fast Fourier Transform)(see Fig33). Next, We got distribution of amplitude value channel by channel and frequency by frequency. Fig33 shows an example. In this event, amplitude is 200 about 400 [kHz] in 10 channel. After repeating this procedure, we could obtain histograms of amplitude value channel by channel, frequency by frequency(34). We used these histograms to reproduce realistic noise. Details are described in the next section

6.5.2. Making FFT noise

The procedure of making FFT noise is below:

1. Get amplitude from the histograms of amplitude at random.
2. Perform Inverse FFT

After performing inverse FFT, there is random noise (Fig35)which have the same distribution of frequency as real data. Real DATA have coherent noise but random noise don't have coherent components, therefore adding coherent components is necessary to reproduce realistic noise.

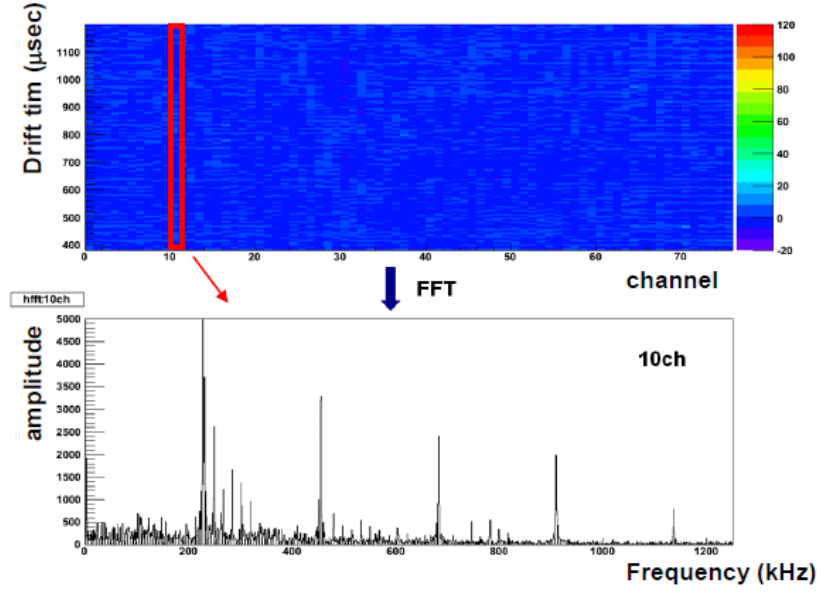


Figure 33: example distribution of frequency:10ch

3. Select random noise 0 and 31 and 63ch
4. Insert random noise 0 ch to 1-30ch, 31ch to 32-62ch, 63ch to 64-75ch
5. Scaling each channel

Real DATA look having coherent noise board by board(We used 3 readout board in T32 experiment). We chosen 3 random noise(0ch,31ch,63ch) in this reason. After that, each channel needs to be corrected as each noise scale. Fig36 shows coherent noise after scaling as Fig37. Vertical axis of Fig37 is RMS of FADC, it stands for noise level.

6.Mixing Random noise and Coherent noise.

Finally, We mixed Random noise and coherent noise as

$$RealisticNoise = RandomNoise + CoherentNoise * 0.5 \quad (2)$$

- Plot: simulated event (Nagasaka)

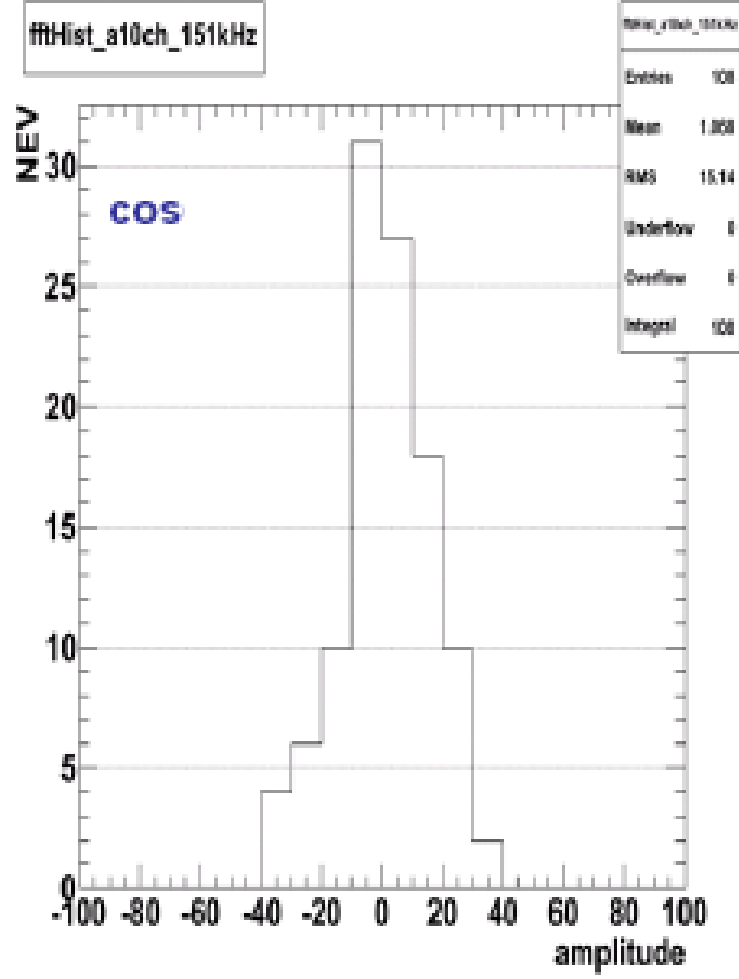


Figure 34: An example of distribution of amplitude

6.6. Cross Talk

We noticed strange shape of integrated ADC distribution of stopped channel as the left of figure38 shows. First, we think this is the leak of signal drifted ionization electrons. However, The shape Monte Carlo Simulation make is very differnt from the shape of DATA. There we look the signal wave form after FFT cut. Then, the signal wave form of events which make the mountain at small integrated ADC is a diffrential of the gaussian shape of stopped channel-1 Figure38 shows the signal wave form of stopped channel

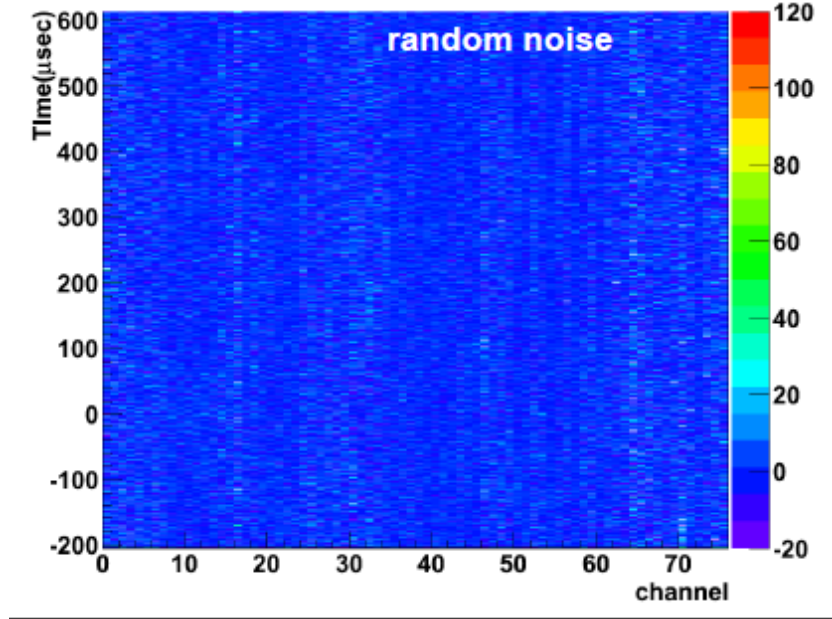


Figure 35: Random noise

and stopped channel-1. This shape is appeared at channel number 1 which cannot enter drifted ionization electron in electric power lines. From here this bipolar shape is what the voltage change of adjacent channels induced. This is remarkably looked stopped channel as stopped channel-1 have large integrated ADC. We implement this crosstalk phenomenon in Monte Carlo Simulation by adding bipolar shape of the signal gaussian shape at adjacent channels. The area of positive region of bipolar shape is 10.5% of the area of gaussian at adjacent channels. The value of 10.5% is determined by comparing the distribution of integrated ADC at stopped channel between DATA and MC. The result of comparison of the distribution is shown in section 7.2.

- Plot: signal waveform (proton stopped point + 1) (A. Okamoto)
- Plot: simulated event with and without cross talk (A. Okamoto)

6.7. Signal and Noise Scale Tuning

- Plot: Landau distribution after the tuning (Tanaka)

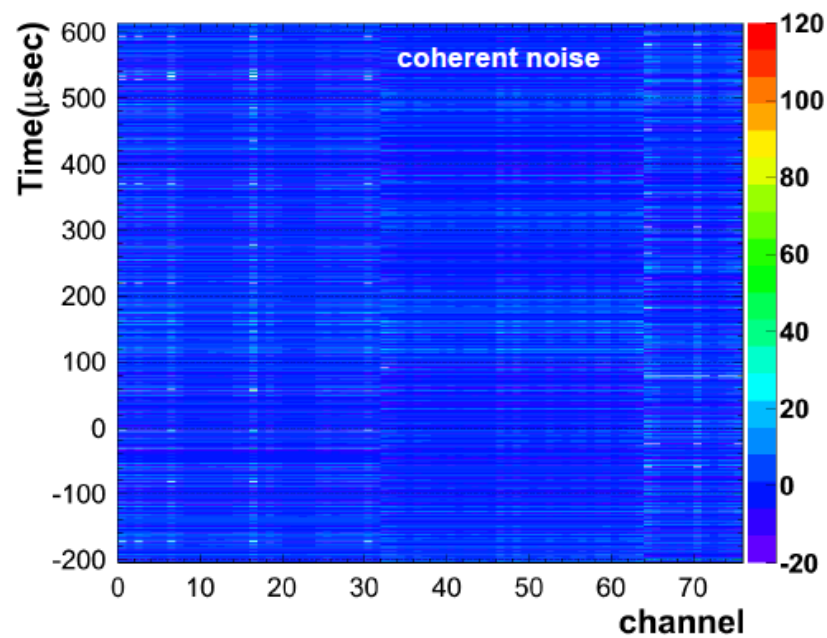


Figure 36: Coherent noise

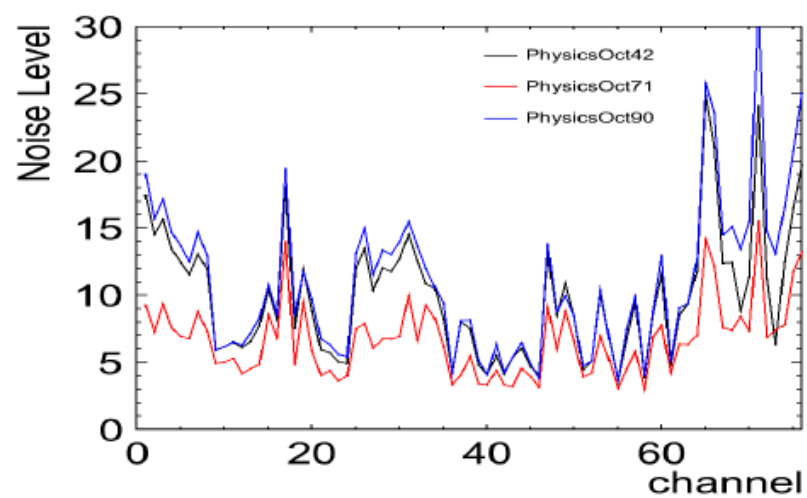


Figure 37: Noise level

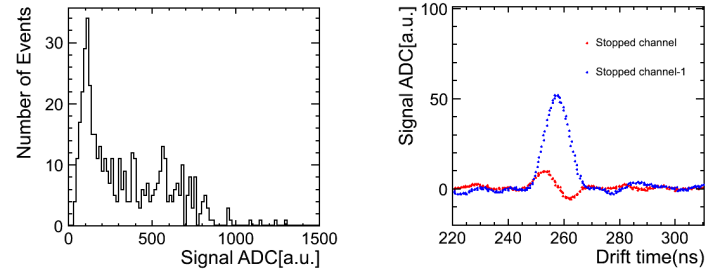


Figure 38: Left: Integrated ADC distribution of stopped channel, Right: Signal wave form of stopped channel

7. Data- MC Comparison

7.1. Through-going Pion

- Plot: Data-MC comparison (Tanaka)

7.2. Stopped Proton

When we indicate the validity of charge response in high dE/dx region, proton is good sample due to its simple event structure. At the same time, we verificate the recombination factor by proton in this analysis because proton has wide dE/dx range, and this is meaningless if the charge response of MC doesn't agree with that of DATA. Therefore proton is very impotant in terms of comprehension of charge response.

Figure?? shows the comparison of the distribution of Hit Charge, Hit Sigma, Stopped Channel and Cluster Charge between DATA and MC. Hit Charge shows the distribution of the integral which fit signal wave form with gaussian. Hit Sigma shows the distribution of all the dispersion which fit signal wave form with gaussian. Cluster Charge shows the sum of the Hit integral of the cluster which is selected as good proton event. All four distribution of MC reproduce DATA well. Especially, the agreement of stopped channel distribution indicates the success of the momentum estimation by TOF information because where proton stopped depends on the initial momentum.

Figure40 shows the integrated ADC distribution of each channel from stopped channel. Crosstalk scale is determined by DATA-MC comparison of the left upper histogram, and this MC distribution agree with DATA well. The MC distribution of the channels after stopped channel are good agreements with DATA.

The left of figure41 shows the mean of the above distribution of each channel. The right of figure41 shows the ratios of DATA/MC. The ratios are surpressed within 92%~100%. From this result, we succeed in reproducing the charge response of DATA in high and wide dE/dx region.

7.3. Stopped Kaon

7.4. Recombination Factor

Electron-ion recombination depends on the electric field and stopping power dE/dx . We have studied this factor using tagged proton beam. Recombination factor measurement using proton beam is relatively easy because of stability of proton. This is why we used proton beam for this study as a

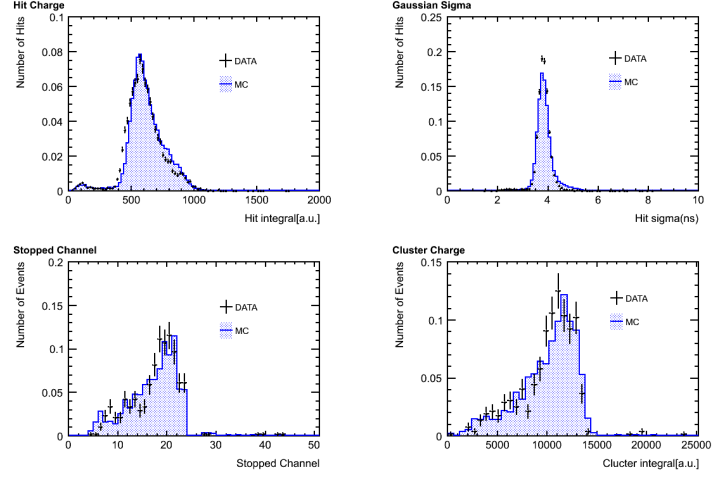


Figure 39: DATA-MC comparison of Hit Charge, Hit Sigma, Stopped Channel, Cluster Charge

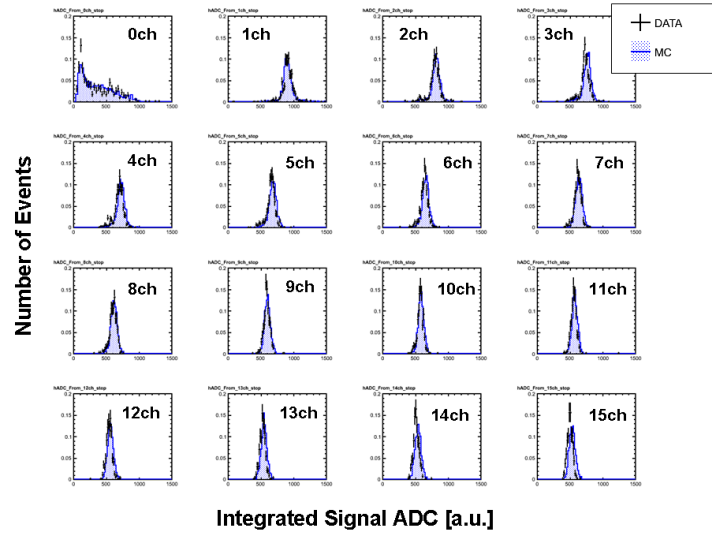


Figure 40: Integrated ADC distribution of each channel from stopped channel

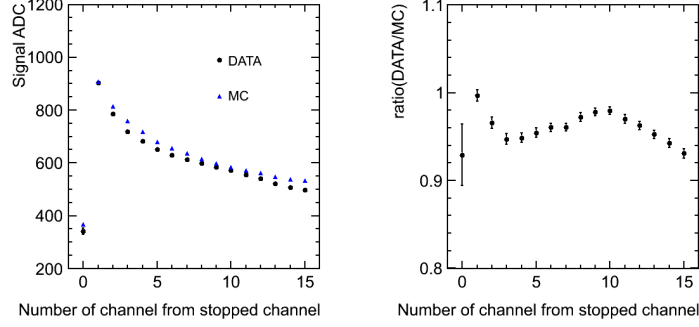


Figure 41: DATA-MC comparison of the mean of Integrated ADC distribution

first step.

Expression for recombination can be derived

$$Q = A \frac{Q_0}{1 + (k/E) \times (dE/dx) \times (1/\rho)} \quad (3)$$

where Q_0 is initial ionization charge, E is electric field, dE/dx is energy deposit per distance, ρ is density of liquid Argon, A and k are fit parameters. This formula can be rearranged like below:

$$\frac{Q_0}{Q} = \frac{1}{A} + \frac{(k/E)(dE/dx)(1/\rho)}{A} \quad (4)$$

The ratio of Q_0/Q depends on stopping power dE/dx , so we determined fit parameter A and k using proton data and Monte Carlo simulation. In this analysis, we need Q , Q_0 and dE/dx channel by channel. First, Electric Field E is fixed at 0.196 [kV/cm]. Second, Q is integrated charge in an anode readout channel. we can get this value from Real DATA. Third, Q_0 is integrated charge without recombination factor in an anode readout channel. This value can be obtained using Qscan. And then, dE/dx per an anode channel is determined with truth information of Qscan MC. Fig42, 43, 44 shows Q , Q_0 , $dEdx$ from stopped channel -1 to stopped channel -14. In many case, integrated charge in stopped channel are composed of cross talk. This is the reason why we don't use information from stopped channel in this analysis.

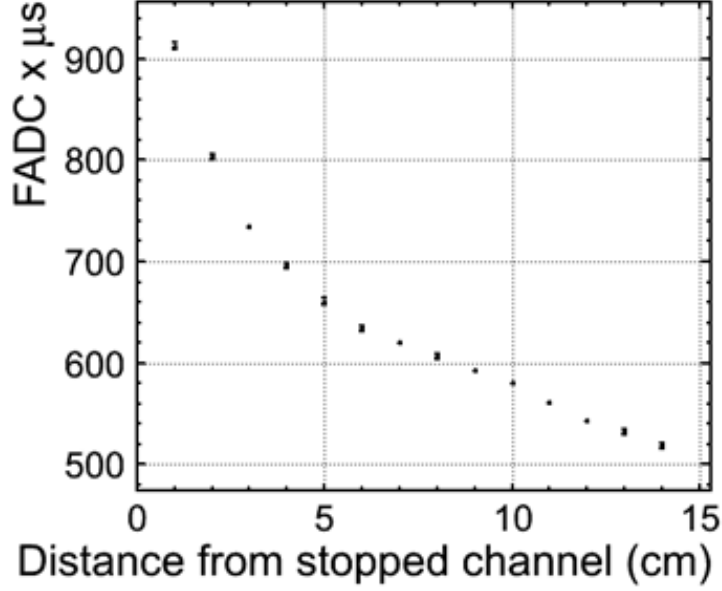


Figure 42: DATA: Integrated Flash ADC counts from stopped channel -1

The result of this study is shown in Fig45. Vertical axis is Q_0/Q , and horizontal axis is dE/dx in this figure, this plot is fitted by Birk's low. As a result, we got fitting parameter

$$\begin{aligned}
 A &= 0.782 \pm 0.009 \\
 k &= 0.0467 \pm 0.0009 [kV(g/cm^2)/cm/MeV]
 \end{aligned} \tag{5}$$

We checked Birk's low in the range $4 [MeV/(g/cm^2)] \leq dE/dx \leq 12 [MeV/cm^2]$ and the result is consistent with ICARUS experiment's one in \sim sigma.

7.5. Stopped Kaon

In this section , we compare some quantities of data and MC simulation that K stop in the liquid argon detector and can detect stopped point. Figure 46 shows Data and MC comprison for signal hit charge , signal width , cluster charge and primary paricle charge distribution. Data of signal charge and signal width are consistnt with MC one in error by less than two % and data

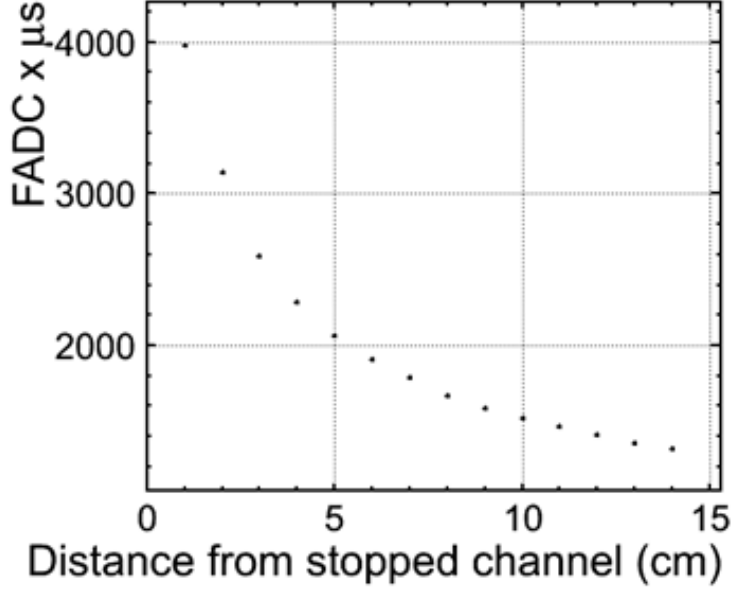


Figure 43: MC without recombination: Integrated Flash ADC counts from stopped channel -1

of cluster charge and primary charge are consistent with MC one in error by less than five %.

Figure 7.5 shows signal hit charge distribution of restricted channel 27. As it can be noticed for figure 7.5, signal charge has two peaks at 300 and 500 dQ/dx. Because two peaks have correlation of Δ TOF, there is some possibility of not passing in the center of the detector. So, we use only the event that signal charge of restricted channel 27 is less than 350. Figure 48 shows signal hit charge distribution in different distance from the stopped point.

As it can be noticed for figure 48, data plot is consistent with MC one. Figure 50 shows data/MC ratio of signal hit charge distribution in different distance from the stopped point. Data of signal charge in different distance from stopped point are consistent with MC one in error by less than five %.

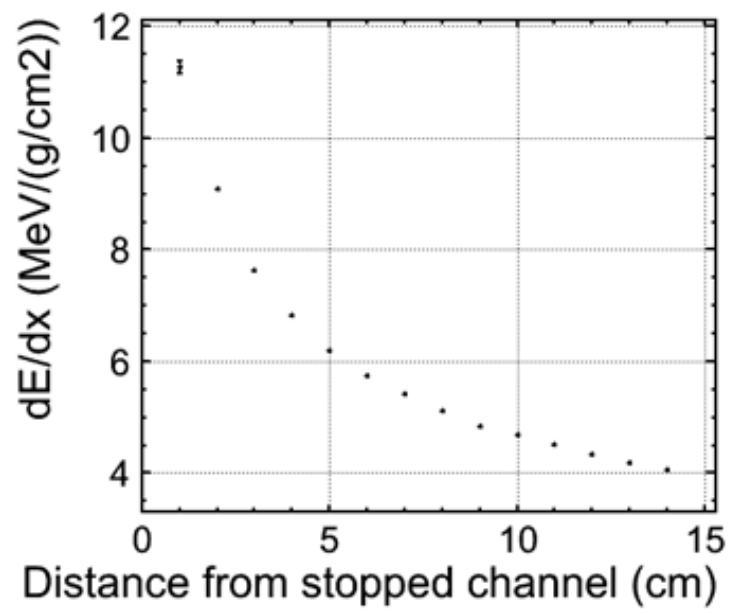


Figure 44: dE/dx from stopped channel -1

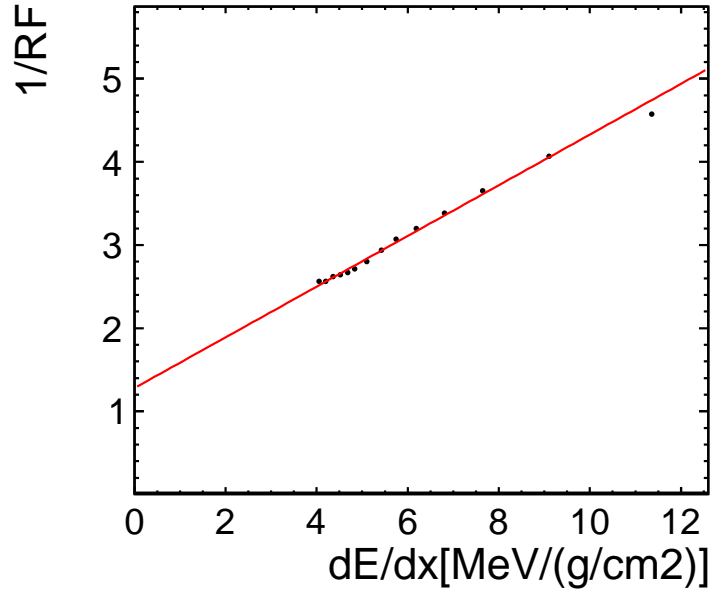


Figure 45: $1/RF$ VS dE/dx : fitted by Birk's law

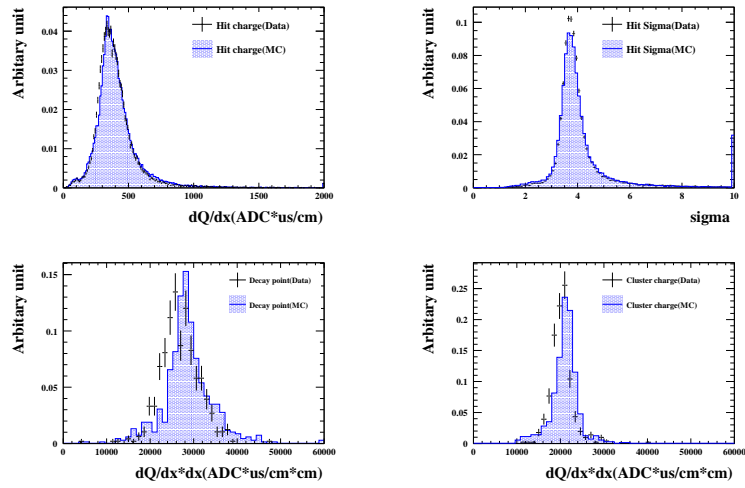


Figure 46: Data-MC comparison for hit charge, hit sigma, cluster charge, primary particle charge

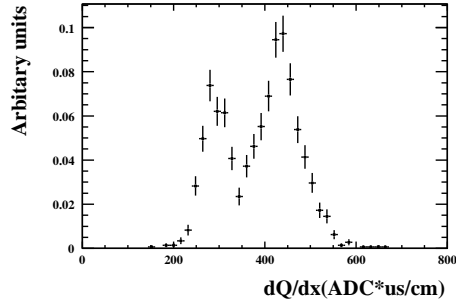


Figure 47: Hit charge in channel 27

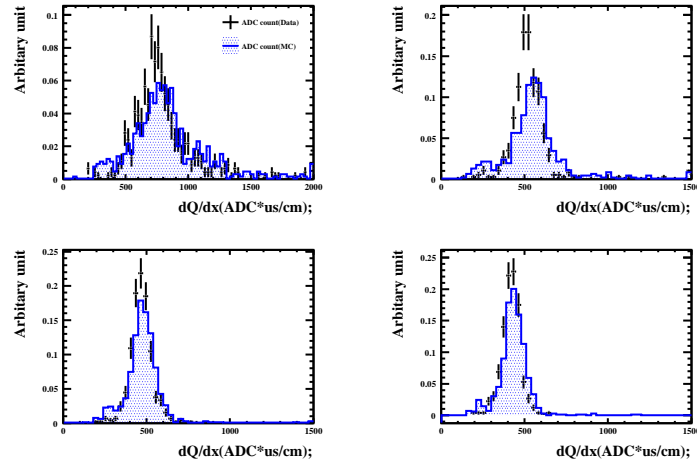


Figure 48: Data-MC comparison for hit charge distribution in different distance from the stopped point(top left:decay point,top light:decay point-5cm,bottom left:decay point-10cm,decay point-15cm)

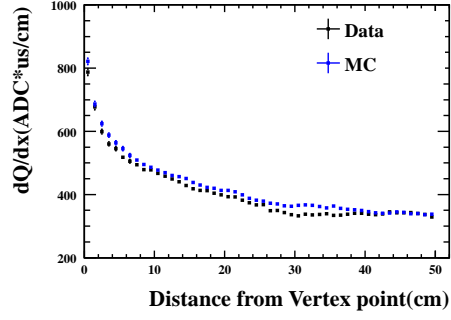


Figure 49: Data-MC comparison for hit charge distribution in different distance from the stopped point

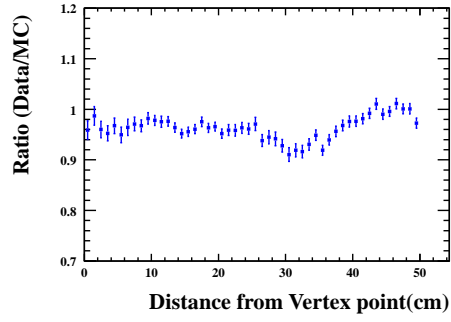


Figure 50: Data/MC ratio for hit charge distribution in different distance from the stopped point

8. Summary

References

- [1] O. Araoka *et al.*, J. Phys. Conf. Ser. **308**, 012008 (2011) [arXiv:1105.5818 [physics.ins-det]].
- [2] S. Mihara [MEG Collaboration], Nucl. Instrum. Meth. A **518**, 45 (2004).
- [3] S. Amoruso *et al.* [ICARUS Collaboration], Nucl. Instrum. Meth. A **523**, 275 (2004).
- [4] S. Amoruso, M. Antonello, P. Aprili, F. Arneodo, A. Badertscher, B. Baibusinov, M. Baldo-Ceolin and G. Battistoni *et al.*, Nucl. Instrum. Meth. A **516**, 68 (2004).
- [5] A. Bettini *et al.*, Nucl. Instrum. Meth. A **305**, 1991 (1991).
- [6] P.V.C Hough 'Method and means for recognizing complex patterns', United States Patent Office 3069654(1962)